Astron. Astrophys. 323, 363–373 (1997)

ASTRONOMY
AND
ASTROPHYSICS

Bar strength and star formation activity in late-type barred galaxies

L. Martinet and D. Friedli⋆

Observatoire de Genève, CH-1290 Sauverny, Switzerland (Louis.Martinet@obs.unige.ch)

Received 23 September 1996 / Accepted 20 December 1996

Abstract. With the prime aim of better probing and understanding the intimate link between star formation activity and the presence of bars, a representative sample of 32 non-interacting late-type galaxies with well-determined bar properties has been selected. We show that all the galaxies displaying the highest current star forming activity have both strong and long bars. Conversely not all strong and long bars are intensively creating stars. Except for two cases, strong bars are in fact long as well. Numerical simulations allow to understand these observational facts as well as the connection between bar axis ratio, star formation activity, and chemical abundance gradient: Very young strong bars are first characterized by a raging episode of star formation and two different radial gaseous abundance gradients, one steep in the bar and one shallow in the disc. Then, principally due to gas consumption, galaxies progressively fall back in a more quiescent state with a nearly flat abundance gradient across the whole galaxy. On the contrary, weak bars are unable to trigger significant star formation or to generate flat abundance gradients. The selected galaxies have tentatively been classified in four classes corresponding to main stages of secular evolution scenario.

Key words: galaxies: abundances – galaxies: evolution – galaxies: starburst – galaxies: structure – infrared: galaxies

1. Introduction

Many clues of secular dynamical evolution in disc galaxies have recently been detected by observations or suggested by numerical simulations and theoretical approaches. The most significant progresses in the field has come from considerations of facts neglected or not well understood in the past. For instance, the role of gas, the effects of interactions not only between galaxies but also between various components of a given system, the necessity to fully take into account 3D structures, the interplay between star formation and dynamical mechanisms, etc. In fact, discs are the seat of evolutionary processes on timescales of the order of the Hubble time or less (see the reviews by Kormendy 1982; Martinet 1995; Pfenniger 1996; see also e.g. Pfenniger & Norman 1990; Friedli & Benz 1993, 1995; Courteau et al. 1996; Norman et al. 1996). In particular, bars do play a decisive role in such processes.

The presence of non-axisymmetric components seems to be a necessary condition for the onset of nuclear activity (Moles et al. 1995). However, the precise link between the presence of stellar bars and the star formation activity is not well established and even somewhat controversial (see e.g. Hawarden et al. 1996). Some authors claimed that star formation is enhanced in barred galaxies (Hawarden et al. 1986; Dressel 1988; Arsenault 1989; Huang et al. 1996), whereas others suggested that barred galaxies have star formation levels similar or lower than those in normal spirals (Pompea & Rieke 1990; Isobe & Feigelson 1992). For instance, according to Hawarden et al. (1986), more than one third of SB galaxies have 25 μm excess attributed to vigorous star formation in a circumnuclear ring located near the inner Lindblad resonance. However, this result generates many unanswered questions: Why do the other galaxies show no significant excess of star formation activity? Is the star formation enhancement dependent on the Hubble type as well? Is the 25 μm excess a reliable indicator of star formation? Where are the preferential sites of star formation located? Etc.

The aim of the present paper is threefold: 1) To quantitatively confirm through observational data from the literature that the strength and/or the length of a bar is a decisive factor for enhancing star formation activity as suggested by numerical simulations (e.g. Friedli & Benz 1993, 1995), observations (Martin 1995), as well as by our preliminary study (Friedli & Martinet 1996). 2) To re-discuss the influence of the bar strength and the star formation efficiency on the radial chemical gradient in the continuation of the work by Martin & Roy (1994). 3) To suggest steps of evolution in barred galaxies taking into account the various points previously mentioned.

This paper is structured as follows: In Sect. 2, we discuss various indicators and estimators of star formation usually considered in the literature, whereas the selection of galaxies used in

Send offprint requests to: L. Martinet

⋆ Present address: Département de physique, Université Laval, Ste-Foy, QC, G1K 7P4, Canada; dfriedli@phy.ulaval.ca

this study is given in Sect. 3. Section 4 is devoted to the presentation of the various links found in our sample between observed quantities, like bar axis ratio, bar length and star formation activity as well as by considering a simple theoretical model able to link the radial abundance gradient, the bar strength, and the star formation efficiency. In Sect. 5 some other jigsaw pieces have been inserted thanks to a new set of numerical simulations. In Sect. 6, we discuss and put the previous results in the general frame of secular evolution of disc galaxies, and finally we summarize our main conclusions in Sect. 7.

2. Star formation activity

2.1. Star formation tracers

There does not seem to exist any observational quantitative estimator of active star formation devoid of ambiguity. The present situation is briefly discussed and summarized in the following four subsections, whereas our final choice is discussed in the fifth one.

2.1.1. Hα

One can expect that Hα emission leads to a good estimator of instantaneous star formation rate (SFR) insofar as it can be checked that they have been corrected for extinction, for instance by comparing with thermal radio luminosities (Sauvage & Thuan 1992). The reader is referred to Kennicutt (1983), Kennicutt & Kent (1983), Keel (1983), and Pogge (1989) for data on the Hα emission properties of normal galaxies. For a general discussion see Kennicutt (1989).

2.1.2. UV

UV fluxes in a bandpass of about 125Å centered at 2000Å have been used by Donas et al. (1987) to obtain quantitative estimates of the current SFR. Difficulties and uncertainties in the correction for extinction are similar to those present for the Hα data.

2.1.3. FIR

The connection between IRAS far-infrared (FIR) and Hα emissions is still controversial. Sauvage & Thuan (1992) outline the strong linearity in a $\log(L_{\mathrm{H}\alpha}) - \log(L_{\mathrm{FIR}})$ correlation. They show that the decrease of the $L_{\mathrm{FIR}}/L_{\mathrm{H}\alpha}$ ratio along the Hubble sequence can be explained by a model of FIR-emitting ISM consisting of two components, i.e. star forming regions and quiescent cirrus-like regions as originally introduced by Lonsdale Persson & Helou (1987) and Rowan-Robinson & Crawford (1989).

Comparing these last approaches, we observe that in two-colour diagram $\log(S_{60}/S_{100})$ versus $\log(S_{12}/S_{25})$, galaxies with $\log(S_{60}/S_{100}) > -0.30$ and $\log(S_{12}/S_{25}) < -0.35$ have a probable contribution to the flux from recent star formation at least of the order of 50%. Moreover, Sauvage & Thuan (1992) infer from the decreasing fraction of L_{FIR} associated to the cirrus from Sa to Sdm that the high mass star formation efficiency increases toward late spiral types. This efficiency is defined as the fraction of FIR-emitting ISM directly associated with star formation.

Various authors directly used FIR colour indices as estimators of current star formation activity. According to Puxley et al. (1988) galaxies with $\log(S_{12}/S_{25}) < -0.35$ are believed to contain regions of star formation. Eskridge & Pogge (1991) admit that $\log(S_{60}/S_{100}) \approx -0.35$ is the value above which a major part of the FIR emission is expected to be due to star formation. Sekiguchi (1987) indicates that the fraction of 60 μm emission attributable to a warm component can be used as an indicator of star formation activity. Dultzin-Hacyan et al. (1990) consider that the best IRAS tracer of recent star formation is the ratio $\log(S_{25}/S_{100})$. In normal galaxies, the mean value of this ratio is -1.30, whereas for liners and starbursts it is respectively -1.15 and -0.75. Moreover, considering ΔHα, the global to central Hα flux ratio taken from Kennicutt (1983) and Keel (1983), we observe a correlation between ΔHα and $\log(S_{25}/S_{100})$. This clearly suggests that some information on star formation activity is contained in this indicator in spite of the caveats mentioned above.

From the analysis of these different suggestions, we can admit that objects for which most of the FIR emission is due to current star formation are separated from those with FIR colours indistinguishable from galactic cirrus by the alternative conditions: $\log(S_{12}/S_{25}) \lesssim -0.35$, $\log(S_{60}/S_{100}) \gtrsim -0.35$, $\log(S_{25}/S_{100}) \gtrsim -1.15$, or $\log(S_{25}^2/S_{12}S_{100}) \gtrsim -0.80$. The ratio α_2/α_1 of the respective contributions of starburst and cirrus in the observed spectrum of IRAS galaxies (Rowan-Robinson & Crawford 1989) could also be considered. The frontier in color indices defined above corresponds to $\alpha_2/\alpha_1 \approx 1$.

Finally, in view of strengthening our statement, we can compare the global values of estimators for various galaxies with local values obtained in nearby galaxies. In fact, the FIR sources in M31 seem to coincide with giant HII regions complexes (Xu & Helou 1996). The same observation is reported by Rice et al. (1990) from IRAS maps of M33 or by Xu et al. (1992) for the LMC. Tomita et al. (1996) localize galaxies in different part of the $\log(S_{100}/S_{60})$ versus $L_{\mathrm{FIR}}/L_{\mathrm{B}}$ diagram corresponding to HII regions, non-HII regions and central regions of M31. This approach suggests that $L_{\mathrm{FIR}}/L_{\mathrm{B}}$ could be a useful indicator of current versus recent star formation rates.

2.1.4. Radio

The origin of the tight correlation between the FIR and the radio continuum emission of late-type galaxies has been discussed by various authors (e.g. Helou 1991 for a review). The 60 μm to 20 cm IR-to-radio ratio seems to be a signature of star formation activity resulting from stars with $m_* \gtrsim 5\,\mathrm{M}_\odot$. As shown by Puxley et al. (1988), the majority of SB galaxies with $\log(S_{12}/S_{25}) < -0.35$ have central radio source emission arising from the center of a burst of star formation. However, such

an emission could also be powered by a density enhancement or a darkened active nucleus.

2.1.5. Our choice

The necessity to have a sample of galaxies as large as possible with both data on bar morphology and star formation activity leads us to prefer FIR to Hα or radio data. We also have to take into account all the different caveats and problems listed in Sect. 2.1.3. Therefore, after having consulted various sources of data, we choose to use $\log(S_{25}/S_{100})$ as indicator of star formation activity for the late-type SBs galaxies from Martin's catalogue (Martin 1995). The effects observed are qualitatively confirmed by using other color indices.

2.2. Star formation rates

For the sake of comparison with numerical simulations (see Sect. 5), we would like to have estimates of the SFRs. However, the SFR values calculated from $L_{\rm FIR}$ data must be used with caution. The results are strongly affected by at least three factors: 1) The choice of the shape and the mass range for the IMF. 2) The IR wavelength range used in published data. 3) The cirrus contribution to $L_{\rm FIR}$ as a function of Hubble type.

Concerning the IMF, it must be emphasized that in the general relation $\mathrm{SFR_{FIR}} = kL_{\rm FIR}$, the value of k will strongly vary depending on the IMF. For instance, for a Salpeter IMF with mass ranges 0.1 – 60 $\mathrm{M_\odot}$, 2 – 60 $\mathrm{M_\odot}$, 8 – 60 $\mathrm{M_\odot}$, k will respectively be $6\cdot10^{-10}$, $3\cdot10^{-10}$, and $1\cdot10^{-10}$ (Telesco 1988). The reality of a top-heavy IMF for starburst galaxies is still debated (see e.g. Sommer-Larsen 1996).

The main source of data for $L_{\rm FIR}$ still come from IRAS fluxes which do not cover the whole IR spectrum. Some extrapolations have been tried to correct for missed fluxes beyond 120 μm and shortward 40 μm. This correction depends on the ratio S_{60}/S_{100} (see e.g. Young et al. 1989).

Finally, the percentage coming from the cirrus contribution can be accounted for by using the two-component model introduced by Lonsdale Persson & Helou (1987). Following Sauvage & Thuan (1994), a contribution of 77% for Sbc's, 70% for Sc's, and 45% for Scd's is adopted.

The previous considerations mean that only relative SFRs are really relevant although access to absolute SFRs remains necessary. Assuming the same IMF for all galaxies in the sample and a linear relation between the FIR flux and the SFR, we use the following relation inferred from Telesco (1988):

$$\mathrm{SFR_{FIR}}[\mathrm{M_\odot\ yr^{-1}}] = 6\cdot10^{-10}\tilde{L}_{\rm FIR}[\mathrm{L_\odot}]\,, \qquad (1)$$

where $\tilde{L}_{\rm FIR}$ is $L_{\rm FIR}$ taken on the 1 – 500 μm range from Young et al. (1989), corrected for the cirrus contribution according to Sauvage & Thuan (1994). Equation 1 concerns the mass range 0.1 – 60 $\mathrm{M_\odot}$. The numerical coefficient must be divided by two if the mass range is 2 – 60 $\mathrm{M_\odot}$ as mentioned before. We introduce a normalizing factor $\overline{\mathrm{SFR}}_{\rm FIR} = 0.72\,\mathrm{M_\odot\ yr^{-1}}$ obtained by inserting into Eq. 1 the mean FIR luminosity for normal Sc galaxies, i.e. $\overline{L}_{\rm FIR} = 4\cdot10^9\,\mathrm{L_\odot}$ (Becklin 1986). Then, we relate all the SFRs to $\overline{\mathrm{SFR}}_{\rm FIR}$,

$$f \equiv \frac{\mathrm{SFR_{FIR}(galaxy)}}{\overline{\mathrm{SFR}}_{\rm FIR}} = C\,\frac{L_{\rm FIR}(\mathrm{galaxy})}{\overline{L}_{\rm FIR}}\,, \qquad (2)$$

where C is a weighting factor to take into account the respective cirrus contribution ($C = 0.77$ for Sbc's; $C = 1.00$ for Sc's; $C = 1.83$ for Scd's). Both f and $\mathrm{SFR_{FIR}}$ are given in Table 1.

For some galaxies in our sample, the SFR deduced from the Hα emission, $\mathrm{SFR_{H\alpha}}$, has been given by Kennicutt (1983) and is also indicated in Table 1. As noted by the author, the individual entries probably possess uncertainties of the order $\pm$50% due to variable extinction. The $\mathrm{SFR_{H\alpha}}$ is not directly comparable to f. However, for our purpose we can be satisfied when observing a qualitative agreement on high and low values of the SFR inferred from FIR and Hα data. Using the same assumptions for the IMF, the distance, and the corrections for extinction as Kennicutt (1983), the $\mathrm{SFR_{UV}}$ (Donas et al. 1987) are on average larger by a factor 1.2 than the $\mathrm{SFR_{H\alpha}}$ for common objects.

3. The galaxy sample

We have selected all the barred galaxies with 1) bar length L and bar axis ratio (b/a) determined by Martin (1995), and 2) IRAS fluxes from various authors. The basic source is Soifer et al. (1989) which is completed from lists by Rice et al. (1988), Young et al. (1989), or Devereux (1987).

Five early-type (Sa to Sb) and 42 late-type (Sbc to Scd) galaxies in Martin's list have IRAS data. The sample was reduced, using two more selection criteria: 1) Galaxies should not be too inclined so that the deprojected axis ratio $(b/a)_i$ does not deviate too much from the projected value (a difference of 1 ellipticity class as defined by Martin was admitted). 2) Galaxies should be isolated or weakly interacting (no companion detected within $10D_{25}$; no morphological disturbances) in order to clearly separate effects coming from the bar from those generated by interactions. An exception is NGC 5457 which presents some moderate morphological disturbances. Seyfert galaxies have not been excluded from the sample, but only two are present (NGC 1365 and NGC 4051).

We have 32 late-type and only 4 early-type objects left. Arguments from the literature can incite to only consider the late types: Bars in them could have spontaneously formed in discs contrary to bars in early types, induced by interactions, as suggested by Noguchi (1996). In fact, in Sect. 5, we will deal with spontaneous bars. Moreover, Sauvage & Thuan (1994) have found a decreasing contribution of the cirrus component to $L_{\rm FIR}$ toward later types. These issues are still subjects of debate. Moreover, the number of early-types that would otherwise be in our sample is small (4) and their inclusion or exclusion does not affect the results and the conclusions at all (see below), which will be based on a final sample of 32 Sbc–Sc–Scd galaxies.

Available data on radial O/H gradients $d[\mathrm{O/H}]/dR$ have also been collected from various sources but mainly from the tables of Martin & Roy (1994) and Zaritsky et al. (1994).

Table 1. Galaxy sample

Names	$(b/a)_i$	$2L_i/D_{25}$	$\log(S_{25}/S_{100})$	f	$\mathrm{SFR_{FIR}}$	$\mathrm{SFR_{H_\alpha}}$	$d[\mathrm{O/H}]/dR$	Class
(1)	(2)	(3)	(4)	(5)	(6)	(7)	(8)	(9)
NGC 578	0.87	0.09	-1.31 ^{S}					
NGC 1313	0.63	0.12	-1.46 ^{R}				0.000 ^{W}	
NGC 1365	0.51	0.27	-1.20 ^{R}				-0.050 / 0.000 * ^{R}	
NGC 1637	0.52	0.13	-0.98 ^{S}	0.3	0.2	0.9		(IV)
NGC 1784	0.58	0.30	-1.16 ^{D}					
NGC 2997	0.85	0.04	-1.31 ^{R}				-0.093 ^{M_1}	
NGC 3184	0.98	0.09	-1.25 ^{S}	2.2	1.5		-0.101 ^{M_1}	I
NGC 3344	0.86	0.06	-1.33 ^{S}	0.6	0.4		-0.231 ^{Z}	I
NGC 3359	0.32	0.20	-1.45 ^{S}	1.7	1.2		-0.070 / 0.006 * ^{M_2}	IV
NGC 3486	0.74	0.07	-1.69 ^{S}	0.3	0.2	2.2		I
NGC 3686	0.35	0.21	-1.35 ^{D}					
NGC 3726	0.70	0.07	-1.34 ^{S}	1.9	1.3	2.2		I
NGC 3887	0.50	0.24	-1.43 ^{S}	1.2	0.8			IV
NGC 3953	0.89	0.17	-1.40 ^{S}	3.3	2.3			(I)
NGC 3992	0.58	0.30	-1.37 ^{Y}	2.0	1.4			IV
NGC 4051	0.52	0.24	-1.04 ^{S}	0.7	0.5			(IV)
NGC 4123	0.36	0.30	-0.93 ^{S}	1.2	0.8			(IV)
NGC 4303	0.63	0.10	-1.21 ^{S}	7.5	5.3	14.0	-0.073 ^{M_1}	II-III
NGC 4304	0.54	0.34	-1.06 ^{D}					
NGC 4321	0.74	0.12	-1.33 ^{S}	5.7	4.0		-0.035 ^{M_1}	II
NGC 5236	0.38	0.22	-1.03 ^{Y}	13.4	9.4		-0.024 ^{Z}	III
NGC 5248	0.90	0.12	-1.22 ^{S}	5.3	3.7	4.3		II
NGC 5371	0.39	0.18	-1.25 ^{S}	5.6	3.9			III-IV
NGC 5457	0.86	0.05	-1.33 ^{S}	2.5	1.8		-0.109 ^{M_1}	I
NGC 5921	0.34	0.25	-1.26 ^{D}					
NGC 6217	0.40	0.38	-1.03 ^{S}	3.2	2.2	5.4		III-IV
NGC 6384	0.64	0.12	-1.48 ^{Y}	4.0	2.8			(II)
NGC 6744	0.52	0.12	-1.41 ^{R}					
NGC 6946	0.87	0.05	-1.24 ^{Y}	10.0	7.0	3.5	-0.089 ^{M_1}	II
NGC 7479	0.41	0.47	-0.80 ^{S}	17.1	12.0	8.1		III
NGC 7678	0.47	0.23	-1.18 ^{S}	10.9	7.6			(III)
NGC 7741	0.20	0.34	-1.39 ^{Y}	0.8	0.6	1.8		IV

Cols. (2) and (3). From Martin (1995).
Col. (4). From ^{D} → Devereux (1987); ^{R} → Rice et al. (1988); ^{S} → Soifer et al. (1989); ^{Y} → Young et al. (1989).
Col. (5). From Eq. 2.
Col. (6). From Eq. 1 using data by Young et al. (1989).
Col. (7). From Kennicutt (1983).
Col. (8). * → Respective slopes in the bar / in the disc regions. From ^{M_1} → Martin & Roy (1994); ^{M_2} → Martin & Roy (1995); ^{R} → Roy & Walsh (1997); ^{W} → Walsh & Roy (1996); ^{Z} → Zaritsky et al. (1994).
Col. (9). Classes indicated in brackets are uncertain.

The selected galaxies cover nearly two decades in FIR luminosity ($1.1 \cdot 10^9$ to $8.9 \cdot 10^{10}$ $\mathrm{L_\odot}$). NGC 3486 and NGC 7479 are respectively the least and most luminous objects of the sample. The luminosity of NGC 7479 is similar for instance to M82 but nearly two orders of magnitude below Arp 220. Strong starbursts are generally characterized by $L_{\mathrm{FIR}} \gtrsim 10^{11}$ $\mathrm{L_\odot}$ and result from significant interactions.

Without being a strong starburst, NGC 7479 has photometric properties comparable to average values given for "Starburst Nucleus Galaxies" (SBNG) as defined by Balzano (1983) or Coziol et al. (1994). For instance, $\log(S_{25}/S_{100})$ (NGC 7479) = -0.80 very close to the average value -0.75 inferred for SBNGs by Dultzin-Hacyan et al. (1990). By comparison, we have for the three following well-known starbursts:
$\log(S_{25}/S_{100})$ (NGC 253) = -1.10,
$\log(S_{25}/S_{100})$ (NGC 1614) = -0.62,
$\log(S_{25}/S_{100})$ (M82) = -0.68.
Moreover, NGC 7479 has $f = 17.1$, whereas f is respectively 6.6 and 143 for NGC 253 and NGC 1614.

The final sample of galaxies is listed in Table 1. The column entries are as follows:
Col. (1): NGC designation of the galaxy.
Col. (2): Deprojected bar axis ratio.
Col. (3): Deprojected bar length in D_{25} unit.

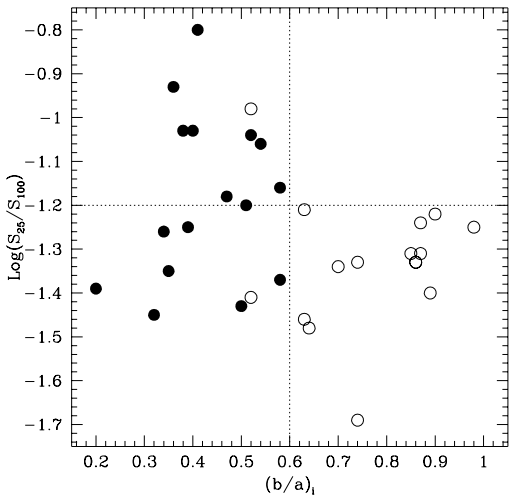

Fig. 1. Relation between the star formation indicator $\log(S_{25}/S_{100})$ and the deprojected bar axis ratio $(b/a)_i$ for the sample of galaxies. Full circles are for long bars ($2L_i/D_{25} \geq 0.18$) and open circles for short bars ($2L_i/D_{25} < 0.18$). Dotted lines separate strong bars from weak ones as well as galaxies actively forming stars from more quiescent ones

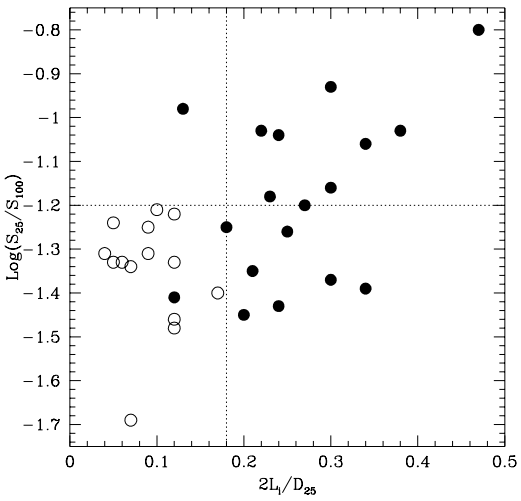

Fig. 2. Relation between the $\log(S_{25}/S_{100})$ and the relative deprojected bar length $2L_i/D_{25}$ for the sample of galaxies. Full circles are for strong bars ($(b/a)_i \leq 0.60$) and open circles for weak bars ($(b/a)_i > 0.60$). Dotted lines separate long bars from short ones as well as galaxies actively forming stars from more quiescent ones

Col. (4): Logarithm of the S_{25}/S_{100} IRAS color index.

Col. (5): Relative star formation rate from FIR data (Eq. 2).

Col. (6): Star formation rate from FIR data (Eq. 1) in $[M_\odot\ yr^{-1}]$.

Col. (7): Star formation rate from Hα emission in $[M_\odot\ yr^{-1}]$.

Col. (8): Radial O/H abundance gradient in $[dex\ kpc^{-1}]$.

Col. (9): Class of the galaxy as defined in Sect. 6.

4. Observed connections

The following subsections discuss the connections or absence of connections between various quantities referring either to the bar morphology, or to the star formation activity, or to abundances indices. Some conventional terminologies are useful. A bar with an axis ratio $(b/a)_i \leq 0.6$ will be called *strong* in the text, whereas the term *weak* will be reserved to bars with $(b/a)_i > 0.6$. Similarly, a bar will be called *long* if its relative length $2L_i/D_{25} \geq 0.18$ and *short* in the opposite case. Finally, we will consider two classes of FIR colours ($\log(S_{25}/S_{100} \geq -1.2$ or $\log(S_{25}/S_{100}) < -1.2$) corresponding to more or less pronounced star formation activity. Clearly, these chosen limits are somewhat arbitrary. However, slight changes of these values do not affect the results presented below. They have been chosen as follows: The axis ratio of 0.6 corresponds to the middle of the interval of observed $(b/a)_i$ values, i.e 0.2 – 1.0. The length of 0.18 separates our sample in roughly half long bars and half short bars. The FIR colour of -1.2 approximately separates systems whose FIR emission is dominated either by star formation from those dominated by cirrus (see Sect. 2.1.3).

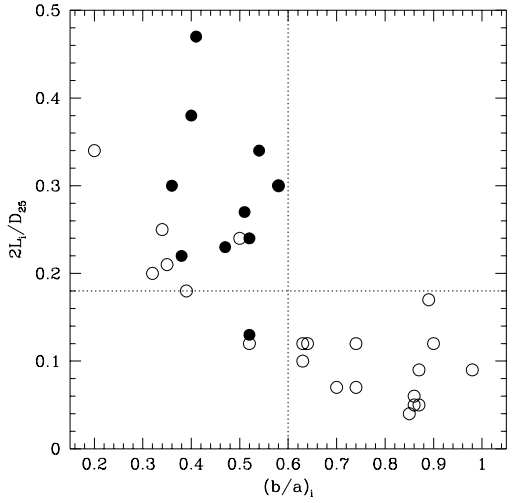

Fig. 3. Relation between $(b/a)_i$ and $2L_i/D_{25}$ for the sample of galaxies. Full circles are for galaxies actively forming stars ($\log(S_{25}/S_{100}) \geq -1.2$) and open circles for more quiescent galaxies ($\log(S_{25}/S_{100}) < -1.2$). Dotted lines separate strong bars from weak ones as well as long bars from short ones

4.1. Star formation activity – bar strength

The link between the $\log(S_{25}/S_{100})$ and the deprojected bar axis ratio $(b/a)_i$ (the bar "strength" parameter) is shown in Fig. 1. In our sample, all the galaxies having $\log(S_{25}/S_{100}) \geq -1.2$ have strong bars (10 galaxies). On the contrary, all the weakly barred galaxies display low current star formation activity (14 galaxies). There are also strongly barred galaxies which do not actively form stars (8 galaxies). These non-active strongly barred galaxies could be either in a "pre-starburst" or in a "post-starburst" phase (see Sect. 5). Using other indicators of star formation activity mentioned in Sect. 2.1.3 (e.g. $\log(S_{25}^2/S_{12}S_{100})$)

does not alter the tendency shown in Fig. 1. With only 32 objects, our statistics is still poor and one should remain cautious before drawing general conclusions. However, in Fig. 1 the different behaviour of weak and strong bars is striking and consistent with the results of numerical simulations presented in Sect. 5. Moreover, Martin (1995) had also noticed that the fraction of strong bars is higher in galaxies with nuclear activity than in quiescent galaxies.

4.2. Star formation activity – bar length

The link between the $\log(S_{25}/S_{100})$ and the relative deprojected bar length $2L_i/D_{25}$ is shown in Fig. 2. All the galaxies but one (NGC 1637) with $\log(S_{25}/S_{100}) \geq -1.2$ have long bars (9 galaxies). This can be explained as follows: Bar-driven movement of gas towards the center takes place inside the co-rotation radius, which is generally close to the end of the bar. Thus in those systems with longer bars, a greater fraction of the total store of gas in the system can be swept up and driven towards the center. Similarly, all the galaxies with a short bar appear to be more quiescent (15 galaxies). However, there are also galaxies with low star formation and long bars (7 galaxies). Thus, the increase of the bar length generally seems to have a similar effect as the decrease of the bar axis ratio.

Surprisingly enough, these two quantities are strongly correlated in our sample (see Fig. 3). Strong bars are long (except NGC 1637 and NGC 6744) and weak bars are short. Whereas it is well-known that on average bars of early-type galaxies are longer than those of late-type galaxies (e.g. Martin 1995), so far no correlation between the length and strength of late-type bars seems to have been highlighted.

4.3. Abundance gradient – bar strength

Martin & Roy (1994) established a correlation between the radial O/H abundance gradient in the discs of SBs and the bar axis ratio (b/a) in the sense that stronger bars have a rather flat gradient, whereas steeper gradients are observed in galaxies with weak or no bars. Taking into account the internal uncertainties and comparing with the data by other authors (e.g. Vila-Costa & Edmunds 1992; Zaritsky et al. 1994), a rather larger dispersion of points in the diagram $\delta_{\rm O} \equiv d[{\rm O/H}]/dR$ versus (b/a) is observed but the above general trend is clearly present.

This suggests that other parameters, such as the efficiency of star formation $\epsilon = L_{\rm FIR}/M_{\rm H_2}$ might play a role in the connection between the chemical and dynamical evolution of bars. According to Tinsley (1980), in a quasi-stationary state the radial chemical gradient essentially depends on the ratio of two timescales, i.e.

$$\frac{d(Z/y)}{dR} \sim -R^{-1}\,\frac{\tau_{\rm in}}{\tau_{\rm sf}}\,, \qquad (3)$$

where $\tau_{\rm in}$ is the characteristic timescale of gas inflow through the center, $\tau_{\rm sf}$ is the characteristic timescale for exhausting gas through star formation, and y is the yield. The extension of this model to the present context suggests that at first approximation $\tau_{\rm in} \sim (b/a)$ since stronger bars have higher gas mass inflow (as shown e.g. by Friedli & Benz 1993). Furthermore $\tau_{\rm sf} \sim \epsilon^{-1}$. So, locally the dependence of the chemical gradient on bar axis ratio must be weighted by the star formation efficiency.

Due to the lack of data in our sample, we must restrict ourselves to register a qualitative agreement between relative observed and calculated gradients for NGC 3344, 4303, 4321, 5236, and 6946. But the real situation can even be more complicated. First, the simplified formula above also shows an R dependence. Second, in some galaxies two different slopes for the O/H abundance gradient have recently clearly been inferred, i.e. NGC 3359 (Martin & Roy 1995) and NGC 1365 (Roy & Walsh 1997). In these two galaxies, the abundance gradient is flat in the disc region, whereas a moderate negative gradient subsists in the bar region (see Table 1). Note that very few galaxies have at least 30 measured HII regions, a necessary condition to be in position to highlight this feature. The numerical simulations reported in Sect. 5 show this feature and indicate that the age of the bar is another factor influencing the chemical gradient.

4.4. Connections with Hubble type

The sample of Table 1 contains late-type galaxies with Hubble types between T=3 and 7. No link has been found between the Hubble type and either $(b/a)_i$, or $2L_i/D_{25}$, or $\log(S_{25}/S_{100})$.

5. Clues from numerical simulations

5.1. Spontaneous bar formation in discs

The most recent ideas concerning the various processes which drive the formation, the evolution and the destruction of bars can be found in the thorough reviews by Sellwood & Wilkinson (1993), Martinet (1995), and Sellwood (1996). Here, only the timescale problem for spontaneous bar formation is briefly discussed.

The details of the formation of galactic discs are still under debate (e.g. Dalcanton et al. 1997), but there are various evidences that their formation could require a non-negligible fraction of Hubble time, or could even be an ongoing process. For instance, various cosmological numerical simulations using the standard CDM scenario indicate timescales of several Gyr for the disc formation (e.g. Steinmetz & Müller 1995). Based on chemical abundance arguments, Sommer-Larsen & Yoshii (1990) also found that continuous infall of proto-galactic material onto the disc over timescales of 4–6 Gyr is necessary. In addition, it is interesting to note that late-type discs appear to be younger than early-type discs (Sommer-Larsen 1996) which suggests that the beginning of the disc assembly might not occur at an universal epoch.

The mechanism of bar formation requires the presence of a well defined disc. The growth of a spontaneous bar may occur in later stages of the disc evolution, i.e. when sufficient gas mass has been accreted onto the disc and, above all, transformed into stars via star formation processes. At some point, the stellar disc will meet the critical conditions necessary for the onset of the bar instability. Star formation works towards this by progressively

adding dynamically cool masses in the stellar disc. For instance, in the models of Noguchi (1996), spontaneous bars typically appear only 6–7 Gyr after the beginning of the disc formation. This is about 10 times longer than the growth of a strong bar (see Sect. 5.3). Thus, the existence of young bars among nearby galaxies is highly expected and very likely observed (Martin & Roy 1995; Martin & Friedli 1997). The fact that barred galaxies seem to be scarce in the Hubble Deep Field (van den Bergh et al. 1996) could also be considered as a possible confirmation of the late appearance of such structures in the life of flattened galaxies. However, this latter study only presents preliminary results which clearly have to be confirmed and interpreted with great care.

5.2. Method, previous and present models

In order to try to explain the observed connection between the bar strength and the SFR presented in the previous section, we have performed a new set of 3D self-consistent numerical simulations with stars, gas, and star formation. Technical details can be found in Pfenniger & Friedli (1993), and Friedli & Benz (1993, 1995). Since our galaxy sample is made of non- or weakly-interacting galaxies, and because the complete process of disc formation is clearly beyond the scope of this paper, we here emphasize some steps of possible evolution implying the mechanism of spontaneous bar formation in an already existing disc.

Previous numerical models (Friedli & Benz 1993) have indicated that the intensity of the gas fueling phenomenon strongly depends on the strength of the bar. As the bar axis ratio (b/a) decreases, much faster gas accumulation into the center occurs. In less than one Gyr, strong bars have nearly pushed all the gas initially inside the bar region into the center, whereas weak bars have only accreted a small fraction of it. The formation of a spontaneous or induced strong bar in a gas-rich Sc-like disc typically triggers a starburst of intermediate power and duration. Depending on the initial amount of gas and the various parameters of the star formation "recipe" (Friedli & Benz 1995), the peak star formation rate is $\approx 8-16\,\mathrm{M}_\odot\,\mathrm{yr}^{-1}$ and the duration is $\approx 0.1-0.2$ Gyr. In particular, stars are formed in gaseous regions unstable with respect to the Toomre parameter (Toomre 1964) $Q_g = s\kappa/\pi G\Sigma_g$, where s is the sound speed, κ is the epicyclic frequency, and Σ_g is the gas surface density. The star formation parameters used in the numerical simulations are not unique but have carefully been chosen in order to reproduce as accurately as possible the observed star formation properties of barred galaxies.

Below, the computed SFR is the mean value over 100 Myr, i.e. from 50 Myr before to 50 Myr after the time at which the corresponding $(b/a)_{\max}$ is determined. This determination was done by applying a standard ellipse-fitting routine to the stellar surface density distribution. The generic model has an initial Sc-like disc with an initial gas to stars mass ratio $M_g/M_* = 0.11$, where M_g is the total gas mass and M_* is the total stellar mass. The value of the Toomre parameter (Toomre 1964) $Q_* = \sigma_R\kappa/3.36G\Sigma_* \approx 1.7$, where σ_R is the radial stellar velocity dispersion, and Σ_* is the stellar surface density. The initial O/H abundance gradient has been set to -0.1 dex kpc^{-1}. In order to smoothly switch on the star formation, the models are first calculated during 400 Myr in a forced axisymmetric state. This procedure also allows us to compute at $t=0$ the SFRs for the corresponding unbarred galaxy. After that, the simulations described below evolve in a fully self-consistent way.

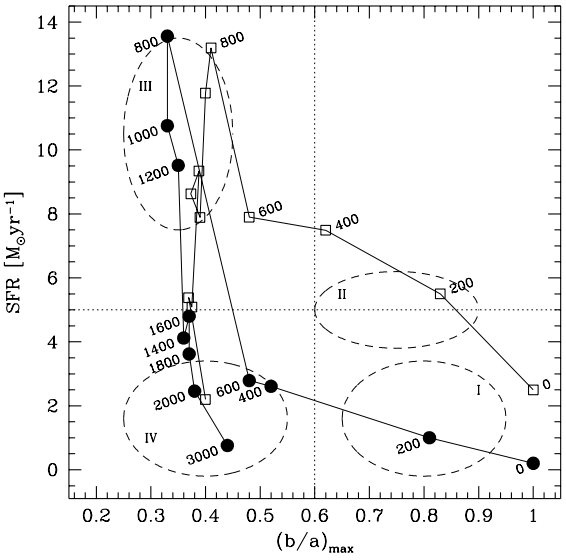

Fig. 4. Time evolution of the total SFR and the maximum bar axis ratio $(b/a)_{\max}$ for typical numerical simulations forming a *strong* bar, either with $M_g/M_* = 0.11$ (full circles; generic model), or with $M_g/M_* = 0.17$ (open squares). The time in Myr is indicated beside symbols when possible. Dotted lines separate strong bars from weak ones as well as galaxies actively forming stars from more quiescent ones. The dashed ellipses schematically indicate the position of the four observational classes defined in Sect. 6

5.3. Strong bar case

For two representative simulations, Fig. 4 shows the time evolution of both the total SFR and the maximum bar axis ratio $(b/a)_{\max}$. As time is evolving, a bar instability progressively develops triggering more star formation. Note that the bar growth and evolution timescales quoted below can be either shorter or longer depending on the instability level of the stellar disc at the beginning of the simulation.

For the generic model at times $t=400$ Myr and $t=600$ Myr, the bar is already strong but the SFR is still modest, mainly concentrated along the bar major axis. This is the "pre-starburst" phase where not enough gas mass has been pushed into the center to exceed the critical gas surface density Σ_c necessary for the onset of star formation. The bar axis ratio is progressively decreasing, whereas the bar length is gradually increasing up to $t \approx 800$ Myr where the bar reaches a quasi-stable state ($(b/a)_{\max} \approx 0.33$). This is the lowest bar axis ratio of the whole simulation and it coincides with the maximum SFR observed ($13.6\,\mathrm{M}_\odot\,\mathrm{yr}^{-1}$) with the star formation essentially concentrated at the center. By $t \approx 1400$ Myr the SFR has become more mod-

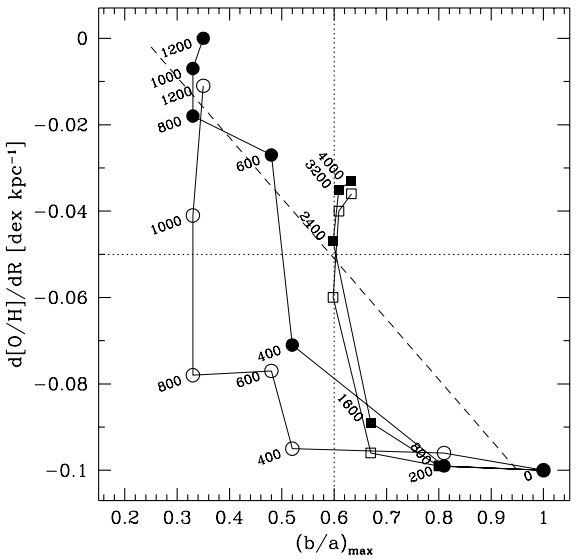

Fig. 5. Time evolution of the O/H abundance gradient $\delta_{\rm O}$ and the maximum bar axis ratio $(b/a)_{\rm max}$. Circles corresponds to the strong bar case (generic model) whereas squares are for the weak bar case. Open and full symbols are respectively for the abundance gradients in the bar (i.e. 2 – 8 kpc) and disc (i.e. 12 – 18 kpc) regions. Both models have M_g/M_* = 0.11. The time in Myr is indicated beside symbols when possible. Dotted lines separate strong bars from weak ones as well as steep abundance gradients from shallow ones. The dashed line corresponds to the observed relation by Martin & Roy (1994)

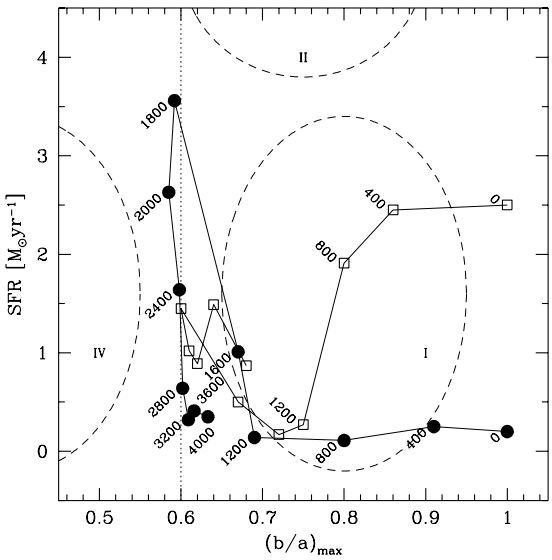

Fig. 6. The same as for Fig. 4 but for typical numerical simulations forming a *weak* bar, either with M_g/M_* = 0.11 (full circles), or with M_g/M_* = 0.17 (open squares). Note the different scales for both axes with respect to Fig. 4

erate once more, although the bar is still strong. This is the beginning of the "post-starburst" phase where the gas has been sufficiently consumed to go again below Σ_c and nearly stop star formation although large amounts of gas remain near the center.

By t = 2000 Myr, the bar axis ratio has increased very slightly ($(b/a)_{\rm max} \approx 0.38$), but the SFR has dropped by a factor of more than 6 (SFR $\approx 2.5\,{\rm M}_\odot\,{\rm yr}^{-1}$). Finally, after one further Gyr, at t = 3000 Myr, the SFR has decreased to less than $1\,{\rm M}_\odot\,{\rm yr}^{-1}$, while the bar has become a little weaker still ($(b/a)_{\rm max} \approx 0.44$). At this time, the total gas to star mass ratio $M_g/M_* \approx 0.04$, and the gas represents less than one percent of the dynamical mass inside 1 kpc.

So, clearly strong bars do not necessarily always host enhanced central star formation. The presence of observed galaxies in the lower left corner of Fig. 1 is thus easily explained. The upper right corner of Fig. 1 cannot be reached and crossed by the generic model. However, one possible way is to strongly increase the gas mass ($M_g/M_* \gtrsim 0.15$) in order to produce a widely over-critical disc of gas with respect to the Toomre criterion. Such discs will form stars at a very high rate whatever the bar strength is, and the formation of a strong bar only results in a moderate increase of the total SFR. As an example, the evolutionary track of a model similar to the generic one but with M_g/M_*=0.17 is also presented in Fig. 4.

For the generic simulation, the time evolution of the radial O/H abundance gradient $\delta_{\rm O}$ and the maximum bar axis ratio $(b/a)_{\rm max}$ is presented in Fig. 5. The time evolution of $\delta_{\rm O}$ in the bar (i.e. 2 – 8 kpc) and disc (i.e. 12 – 18 kpc) regions are both shown. A very different behaviour is observed. The disc abundance gradient becomes very quickly very shallow as soon as the strong bar develops. It moves from -0.10 at t=200 Myr to ≈ -0.02 at t = 800 Myr. On the contrary, the abundance gradient in the bar region remains first steep. It changes from -0.10 at t = 200 Myr to ≈ -0.08 at t = 800 Myr, and only becomes shallower (-0.01) around t = 1200 Myr. Moreover, the galaxy core becomes very oxygen-rich as well.

In the bar region, during the early phase of its existence, the gradient is maintained since the gas dilution (following the significant gas inflow) is compensating for the heavy-element production in the furious star formation then going on in the nuclear vicinity. For more details, see also Friedli et al. (1994), Friedli & Benz (1995), Martin & Friedli (1997). This of course results in the presence of *two different radial abundance gradients in young strongly barred galaxies*. For instance, at t=800 Myr, the slope ratio is about 4.3. After t=1200, the disc abundance gradient remains essentially flat, whereas the lack of gas inside the bar region prevents there any reliable determination of the abundance gradient. So, there is a "steep-shallow" break in the slope profile of $\delta_{\rm O}$ as already observed in at least two galaxies (see Table 1). A "shallow-steep" break could also be present close to the edge of the optical disc (see e.g. Friedli et al. 1994; Roy & Walsh 1997) but it has not yet been observed.

5.4. Weak bar case

Observed weak bars are either i) asymptotically and intrinsically weak, or ii) transient features progressively turned into strong bars as seen in the previous section. In the latter case, the duration of the weak bar phase depends on the timescale of the bar instability growth. This timescale becomes longer if more

of the total mass resides in slow or non-rotating components like massive dark halos or stellar bulges, i.e. the lower values of the Ostriker-Peebles parameter (Ostriker & Peebles 1973). The fact that weak bars are short (see Sect. 4.2) is an indication that they might in fact be growing strong bars. Moreover, it has been proven quite difficult to numerically form permanent, realistic, weak bars. They can however be produced either by putting at the center a "point mass", e.g. a dense cluster or a supermassive black hole with mass $0.01 \lesssim M_{\rm BH}/M_* \lesssim 0.03$ (Friedli 1994; see also Norman et al. 1996), or by increasing the stellar radial velocity dispersion so that $2 \lesssim Q_* \lesssim 3$ (Athanassoula 1983). The presence of large amounts of *highly viscous* gas significantly reduces the maximum bar strength as well (see Figs. 4 and 6).

We chose the method of disc heating. So, the models presented here are similar to the ones of Sect. 5.3 except for the Q_* value which has been increased by 30%, i.e. $Q_* \approx 2.1$. The time evolution of both the total SFR and $(b/a)_{\rm max}$ is shown in Fig. 6. The bar growth timescale is much smaller than for the strong bar case. The spiral arms also remain very weak since the transfer of angular momentum is modest.

For the model with M_g/M_* = 0.11, up to t = 1200 Myr, the SFR is essentially constant and very low ($\approx 0.2\,{\rm M}_\odot\,{\rm yr}^{-1}$), whereas the bar length is gradually increasing and the bar axis ratio is progressively decreasing ($(b/a)_{\rm max} \approx 0.69$). Then, up to t = 2400 Myr, the SFR appreciably increases and the bar becomes a little stronger. The maximum SFR is $\approx 3.6\,{\rm M}_\odot\,{\rm yr}^{-1}$, the star formation being essentially concentrated along the bar major axis and in the center. The lowest bar axis ratio of the whole simulation is $(b/a)_{\rm max} \approx 0.59$ so that this model corresponds in fact to an intermediate case between weak and strong bars. After that, up to t = 4000 Myr, the SFR continues to decrease to reach a quasi-stationary state of $\approx 0.4\,{\rm M}_\odot\,{\rm yr}^{-1}$ whose major contribution comes from a nuclear ring. The bar axis ratio increases up to $(b/a)_{\rm max} \approx 0.63$. At the end of the simulation, $M_g/M_* \approx 0.09$.

The evolution of the model with M_g/M_* = 0.17 is somewhat surprising. Up to t = 800 Myr, the over-critical gaseous disc forms stars at a relatively high rate ($\approx 2.5\,{\rm M}_\odot\,{\rm yr}^{-1}$). Then, the SFR suddenly drops as the disc is progressively becoming self-regulated, i.e. $Q_g \gtrsim 1$ all over the gaseous disc. At t = 2000 Myr, the growth of the weak bar (up to $(b/a)_{\rm max} \approx 0.60$) starts to influence the SFR which increases. However, although high amounts of gas are still present, the peak SFR of this model is smaller by a factor 2.5 than the one of the model with M_g/M_* = 0.11. The efficiency of gas fueling is much reduced since the bar remains short, and its maximum axis ratio gradually increases ($(b/a)_{\rm max} \approx 0.68$ at t = 4000 Myr). Thus, in our models, the increase of the M_g/M_* ratio results in shorter and weaker bars.

The time evolution of $\delta_{\rm O}$ and $(b/a)_{\rm max}$ is presented for both bar and disc regions in Fig. 5. Contrary to the strong bar case, a similar behaviour is observed in these two regions although the abundance gradient remains always a little steeper in the bar (at most by 27%). The abundance gradients essentially remain unchanged up to $t \approx 1600$ Myr where $(b/a)_{\rm max} \approx 0.67$. Then, when $(b/a)_{\rm max} \lesssim 0.6$, they relatively quickly flatten to finally reach a nearly constant value around -0.035 at t = 4000 Myr. This value is slightly larger than the one derived from the observed relation given by Martin & Roy (1994), i.e. $\delta_{\rm O} \approx -0.05$. The relevant points are that, a) weak bars need much longer timescales to flatten radial abundance gradients, b) weak bars are unable to produce totally flat abundance gradients.

Table 2. Characteristics of galaxy class

Parameter	Class I	Class II	Class III	Class IV
Bar strength	weak	weak	strong	strong
SFR	low	median	high	low
f	$\lesssim 3$	$4-10$	$\gtrsim 10$	$\lesssim 2$
$\log(S_{25}/S_{100})$	$\lesssim -1.3$	≈ -1.3	$\gtrsim -1.0$	$\lesssim -1.3$

6. Discussion

In order to quantitatively compare the results of the numerical simulations with the observational features, we have tentatively distinguished in our sample four main classes of late-type objects according to their $(b/a)_i$, SFR/relative SFR (f), and $\log(S_{25}/S_{100})$. We stress that only relative values of the last three parameters are reliable. The respective properties of the four classes have been summarized in Table 2. Clearly the galaxies belonging to these various classes occupy different regions of this 4D parameter space. As can be seen in the suggested classification of Table 1, some galaxies have either intermediate properties between two classes, or half the properties of one class and the other half from another class. Of course, some galaxies cannot be classified due to the lack of data. For the same reason, we decided not to include the abundance gradient as a fifth parameter in this classification.

Class I. Galaxies with large $(b/a)_i$ (0.65 – 0.95), weak SFR ($\lesssim 3\,{\rm M}_\odot\,{\rm yr}^{-1}$), $f \lesssim 3$, and very low values of $\log(S_{25}/S_{100})$ ($\lesssim -1.3$). Typical galaxies of this class are NGC 3344, NGC 3726 and NGC 5457.

Class II. Galaxies are here again characterized by large $(b/a)_i$ (0.60 – 0.90), but much higher SFR ($\approx 4-6\,{\rm M}_\odot\,{\rm yr}^{-1}$), and f (4 – 10). The $\log(S_{25}/S_{100})$ is between -1.2 and -1.3. Representative galaxies of this class are NGC 4321, NGC 5248, and NGC 6946.

Class III. This class includes galaxies with strong bars $(b/a)_i$ (0.25 – 0.45), very high SFR ($\gtrsim 6\,{\rm M}_\odot\,{\rm yr}^{-1}$), $f \gtrsim 10$, and $\log(S_{25}/S_{100}) \gtrsim -1.0$. Two typical objects are NGC 5236 and NGC 7479.

Class IV. As in the previous class, galaxies belonging to this last class have strong bars $(b/a)_i$ (0.25 – 0.55), but much weaker SFR ($\lesssim 3\,{\rm M}_\odot\,{\rm yr}^{-1}$), $f \lesssim 2$, and $\log(S_{25}/S_{100}) \lesssim -1.3$. Prototypes are NGC 3359, NGC 3887 and NGC 7741.

The four SBa–SBb objects initially selected (see Sect. 3) have a strong bar. The value of $\log S_{25}/S_{100}$ for NGC 3351 ($(b/a)_i$ = 0.56) is -1.13. For NGC 7552 ($(b/a)_i$ = 0.29), it is -0.92. Both could be included in class III. NGC 4394 ($(b/a)_i$ = 0.48) and NGC 4725 ($(b/a)_i$ = 0.43) respectively have -1.35

and -1.42. They should belong to class IV. As already noted, they do not modify the discussion in this paper.

Of course, the transition from one class to the other is not instantaneous and some galaxies can populate regions outside the schematic and indicative zones drawn on Figs. 4 and 6. The confrontation with the results from numerical simulations of galaxies developing spontaneous bars clearly suggests possible evolutionary sequences as presented below.

i) Strong bar: When $M_g/M_* \approx 0.1$, the sequence should be [I $\rightarrow$ IV $\rightarrow$ III $\rightarrow$ IV]. In the case where the gas to star mass ratio is higher ($M_g/M_* \gtrsim 0.15$), the evolutionary sequence is [II $\rightarrow$ III $\rightarrow$ IV [1]] instead. A subsequent evolution [IV $\rightarrow$ III] could only be considered if high amounts of fresh gas are provided to the bar over short timescales, i.e. most likely from outside.

ii) Weak bar: The evolution is essentially enclosed in zone [I] irrespective of the gas to star mass ratio. However, when $M_g/M_* \approx 0.1$, a mini-starburst allows the model to come very close to zone [II].

Class IV is hybrid. Indeed, galaxies belonging to this class are either in the "pre-starburst" phase or in the "post-starburst" one. The respective fraction of either type for the late-type galaxies is unknown. However, the "post-starburst" galaxies should certainly be more numerous since the "pre-starburst" phase appears quite short in numerical simulations. There are at least two observational possibilities to distinguish between these two phases. The first one relates to star formation and the second one to abundance gradient. In "pre-starburst" galaxies, star formation is increasing so that current star formation should already be higher than recent star formation. For instance $L_{\rm FIR}/L_{\rm B}$ should be high (Tomita et al. 1996). According to numerical models (Sect. 5), these galaxies show widely different abundance gradients in the bar ($\delta_{\rm O} \rightarrow$ steep) and disc ($\delta_{\rm O} \rightarrow$ shallow) regions. On the contrary, in "post-starburst" galaxies, star formation is strongly declining so that current star formation should already be lower than recent star formation, i.e. $L_{\rm FIR}/L_{\rm B}$ should be low. These galaxies present similar abundance gradients in the bar and disc regions ($\delta_{\rm O} \rightarrow$ flat). For instance in our sample, NGC 3359 has two different radial abundance slopes; this galaxy seems to be in a "pre-starburst" phase and its bar should be young as already suggested by Martin & Roy (1995).

The formation of a spontaneous or induced strong bar in a gas-rich Sc-like disc appears to be a major dynamical event. It results in many secular alterations of the galaxy properties over typical timescales of one tenth of the Hubble time. In this paper, we have mainly focused on bar-induced changes of the star formation (both in spatial distribution and intensity) and the radial gaseous abundance gradient. However, bars are clearly able to deeply reshape the overall morphology, kinematics, and chemistry of disc galaxies on less than a Hubble time as well (see e.g. Martinet 1995).

[1] or even I if central gas accumulation nearly dissolves the bar (see e.g. Friedli & Benz 1993).

7. Conclusions

The main aim of this paper was to improve our understanding of the connection between star formation activity and the presence of bars in spiral galaxies located in regions of low galaxy density. In particular, we intended to explain for what reasons only a fraction of SBs show indices of enhanced star formation activity. Our main results can be summarized as follows:

1) The non-interacting late-type galaxies most active in forming stars have both strong ($b/a \leq 0.6$) and long ($2L_i/D_{25} \geq 0.18$) bars. However, not all strong and long bars are actively creating stars. Weak bars do not display any significant excess of star formation activity. In general strong bars are long as well. Although the sample is too poor to draw definite and more detailed conclusions, the trend outlined here is unquestionable.

2) The selected galaxies have been shared in four distinct classes according to their respective bar strength, $\log(S_{25}/S_{100})$, and relative SFR. During the dynamical evolution, SBs probably go through these classes according to various specific tracks. Numerical simulations enlight possible scenarios. Very young strong bars are first characterized by a vigorous episode of star formation and two different radial gaseous abundance gradients, one steep in the bar and one shallow in the disc. Then, the galaxies progressively fall back in a more quiescent state with a nearly flat abundance gradient across the whole galaxy. On the contrary, weak bars are unable to induce significant star formation or flat abundance gradients.

3) The slope profile of the radial abundance gradient is monitored by: i) The strength of the bar (weak bar $\rightarrow$ slow and moderate modifications of the initial gradient; strong bar $\rightarrow$ quick flattening of the initial gradient). ii) The age of the bar (young bar $\rightarrow$ spatially distinct gradients; old bar $\rightarrow$ single gradient). iii) The spatially-dependent star formation efficiency.

4) For late-type spirals the controversy concerning the role of bars in enhancing/reducing star formation may be resolved if in fact only *young and strong bars enhance star formation*. Larger samples would however be necessary to fully confirm this assertion.

From these conclusions, it clearly appears that the formation of a spontaneous strong bar in an isolated gas-rich Sc-like disc is a major event in the dynamical history of the galaxy. This results in a significant and specific alteration of the spatial distribution and intensity of star formation, as well as of the radial abundance gradients. In particular, some of these remarkable characteristics could help finding young bars.

Finally, some caveats must be mentioned: a) These results only concern isolated late-type spirals. b) We do not take into account possible accretions or interactions which could play a role in the subsequent internal evolution and consequently modify the star formation efficiency, the morphology of bars, and even the Hubble type (Pfenniger 1993). c) The IRAS data do not have a sufficient resolution to allow detailed studies of the star formation morphology, e.g. along the bar or in the nucleus. Generally, the most intense star formation tends to occur in the circumnuclear regions near the ILRs when they exist or in the nuclei when ILRs are absent (see Telesco et al. 1993). Studies

of individual galaxies are still too scarce to allow statistical investigations in such a context. No doubt that ISO data will be most valuable to improve the present situation.

Acknowledgements. This work has been supported by the University of Geneva (Geneva Observatory) and the Swiss National Science Foundation (FNRS). We especially thank D. Pfenniger and J-R. Roy for instructive discussions and a careful reading of the manuscript as well as the referee, T.G. Hawarden, for very useful and detailed comments.

References

Arsenault R., 1989, A&A 217, 66
Athanassoula, L., 1983, in: Internal Kinematics and Dynamics of Galaxies, IAU Symp. No. 100, ed. L. Athanassoula. Reidel, Dordrecht, p. 243
Balzano V.A., 1983, ApJ 268, 602
Becklin E.E., 1986, in: Light on Dark Matter, ed. F.P. Israël. Reidel, Dordrecht, p. 415
Courteau S., de Jong R.S., Broeils A.H., 1996, ApJ 457, L73
Coziol R., Demers S., Pea M., Barneoud R., 1994, AJ 108, 405
Dalcanton J.J, Spergel D.N., Summers F.J., 1997, ApJ, in press
Devereux N., 1987, ApJ 323, 91
Devereux N., Young J.S., 1990, ApJ 350, L25
Donas J., Deharveng J.M., Milliard B., Laget M., Huguenin D., 1987, A&A 180, 12
Dressel L.L., 1988, ApJ 329, L69
Dultzin-Hacyan D., Masegosa J., Moles M., 1990, A&A 238, 28
Eskridge P.B., Pogge R.W., 1991, AJ 101, 2056
Friedli, D., 1994, in: Mass-Transfer Induced Activity in Galaxies, ed. I. Shlosman. Cambridge University Press, Cambridge, p. 268
Friedli D., Benz W., 1993, A&A 268, 65
Friedli D., Benz W., 1995, A&A 301, 649
Friedli D., Benz W., Kennicutt R., 1994, ApJ 430, L105
Friedli D., Martinet L., 1996, in: Starburst Activity in Galaxies, eds. J. Franco et al. RevMexAA (Serie de Conferencias), in press
Hawarden T.G., Mountain C.M., Leggett S.K., Puxley P.J., 1986, MNRAS 221, 41p
Hawarden T.G., Huang J.H., Gu Q.S., 1996, in: Barred Galaxies, eds. R. Buta et al. ASP Conf. Series Vol. 91, p. 54
Huang J.H., Gu Q.S., Su H.J., et al., 1996, A&A 313, 13
Helou G., 1991, in: The Interpretation of Modern Synthesis Observations of Spiral Galaxies, eds. N. Duric, P.C. Crane. ASP Conf. Series Vol. 18, p. 125
Isobe T., Feigelson E.D., 1992, ApJS 79, 197
Keel W.C., 1983, ApJS 52, 229
Kennicutt R.C., 1983, ApJ 272, 54
Kennicutt R.C., 1989, ApJ 344, 685
Kennicutt R.C., Kent S.M., 1983, AJ 88, 1094
Kormendy J.J., 1982, in: Morphology and Dynamics of Galaxies, 12th Advanced Course of the SSAA, eds. L. Martinet, M. Mayor. Geneva Observatory, Geneva, p. 113
Lonsdale Persson C.J., Helou G., 1987, ApJ 314, 513
Martin P., 1995, AJ 109, 2428
Martin P., Friedli D., 1997, A&A, submitted
Martin P., Roy J-R., 1994, ApJ 424, 599
Martin P., Roy J-R., 1995, ApJ 445, 161
Martinet L., 1995, Fund. Cosmic Physics 15, 341
Moles M., Márquez I., Pérez E., 1995, ApJ 438, 604
Noguchi M., 1996, ApJ 469, 605
Norman C.A., Sellwood J.A., Hasan H., 1996, ApJ 462, 114
Ostriker J.P., Peebles P.J.E., 1973, ApJ 186, 467
Pfenniger D., 1993, in: Galactic Bulges, IAU Symp. No. 153, eds. H. Dejonghe, H.J. Habing. Reidel, Dordrecht, p. 387
Pfenniger D., 1996, in: Barred Galaxies and Circumnuclear Activity, Nobel Symp. 98, eds. Aa. Sandqvist, P.O. Lindblad. Lecture Notes in Physics, Vol. 474, Springer, p. 91
Pfenniger D., Friedli D., 1993, A&A 270, 561
Pfenniger, D., Norman, C., 1990, ApJ 363, 391
Pogge R.W., 1989, ApJS 71, 433
Pompea S.M., Rieke G.H., 1990, ApJ 356, 416
Puxley P.J., Hawarden T.G., Mountain C.M., 1988, MNRAS 231, 465
Rice W., Lonsdale C.J., Soifer B.T., et al., 1988, ApJS 68, 91
Rice W., Boulanger F., Viallefond F., et al., 1990, ApJ 358, 418
Rowan-Robinson M., Crawford J., 1989, MNRAS 238, 523
Roy J-R., Walsh J.R., 1997, MNRAS, in press
Sauvage M., Thuan T.X., 1992, ApJ 396, L69
Sauvage M., Thuan T.X., 1994, ApJ 429, 153
Sekiguchi K., 1987, ApJ 316, 145
Sellwood J., 1996, in: Barred Galaxies, IAU Coll. No. 157, eds. R. Buta et al. ASP Conference Series, p. 259
Sellwood J., Wilkinson A., 1993, Rep. Prog. Phys. 56, 173
Soifer B.T., Boehmer L., Neugebauer G., Sanders D.B., 1989, AJ 68, 766
Sommer-Larsen J., 1996, ApJ 457, 118
Sommer-Larsen J., Yoshii Y., 1990, MNRAS 243, 468
Steinmetz M., Müller E., 1995, MNRAS 276, 549
Telesco C.M., 1988, ARA&A 26, 343
Telesco C.M., Dressel L.L., Wolstencroft R.D., 1993, ApJ 414, 120
Tinsley B., 1980, Fund. Cosmic Physics 5, 287
Tomita A., Tomita Y., Saito M., 1996, PASJ 48, 285
Toomre, A., 1964, ApJ 139, 1217
Vila-Costa M.B., Edmunds M.G., 1992, MNRAS 259, 121
van den Bergh S., Abraham R.G., Ellis R.S., et al., 1996, AJ 112, 359
Walsh J.R., Roy J-R., 1997, MNRAS, in press
Xu C., Helou G., 1996, ApJ 456, 152
Xu C., Klein U., Meinert D., et al., 1992, A&A 257, 47
Young J.S., Xie S., Kenney J.D.P., Rice W.L., 1989, ApJS 70, 699
Zaritsky D., Kennicutt R.C., Huchra J.P., 1994, ApJ 420, 87

This article was processed by the author using Springer-Verlag TEX A&A macro package version 4.